LRP 483/93 October 1993

# EFFECT OF THE PARALLEL CURRENT DENSITY ON THE LOCAL IDEAL 3D MHD STABILITY OF HELIAS CONFIGURATION

R. Moeckli & W.A. Cooper

# EFFECT OF THE PARALLEL CURRENT DENSITY ON THE LOCAL IDEAL 3D MHD STABILITY OF HELIAS CONFIGURATION

R. Moeckli and W. A. Cooper

Centre de Recherche en Physique des Plasmas
Association Euratom - Confédération Suisse
Ecole Polytechnique Fédérale de Lausanne
21, Av. des Bains - CH-1007 Lausanne/Switzerland

**Abstract**

We study the local ideal three-dimensional (3D) magnetohydrodynamic (MHD) stability for the Wendelstein 7-X (W 7-X) configuration. We confirm a volume average beta limit of 5% with a nearly optimal pressure profile using two methods to calculate the parallel current density : the magnetic method that uses magnetic information of the configuration (in particular, the condition of charge conservation $\nabla \cdot \mathbf{j} = 0$ is explicitly used in the resolution) and the geometric method that uses the geometry of the configuration itself.

We show that the ballooning stability does not depend on the method of the parallel current calculation. In contrast, the value of Mercier criterion depends sensitively on which method is used. Not only is the geometric method not sensitive to resonant surfaces (in particular, the $\iota_p = 1/6$), but there is a systematic error in the Mercier criterion for nonresonant surfaces when not enough modes are used to calculate the equilibria numerically with a spectral method. However, this systematic error does not change the average beta limit of W 7-X because ballooning stability is more stringent than Mercier stability for this configuration.

## 1 Introduction

The stellarator W 7-X [1] is a configuration of the Helias kind [2] (HELIcal Advanced Stellarator) in which the toroidal plasma equilibrium has some optimized properties. Gardner and Blackwell have shown that in the H1 Heliac configuration, which is close to W 7-X because it has low magnetic shear, the way to calculate the parallel current influences the value of the Mercier criterion [3]. It is therefore important to know if it is also the case for the W 7-X and if this problem applies to ballooning stability as well.

Section 2 contains a description of codes used to calculate the equilibrium and to perform the local stability analysis. A description of the two calculation methods for the parallel current is given in section 3. Section 4 shows marginal beta values for local stability with a nearly optimal pressure profile (see figure 1). This profile becomes marginally stable to localised ideal MHD modes nearly uniformly throughout the plasma. We show that the ballooning stability does not depend on the calculation method in section 5. Problems connected with the Mercier criterion and, in particular, the systematic error in the parallel current when the geometric method is used are treated in section 6. Finally, section 7 contains the conclusions.

# 2 Numerical codes

The calculation of equilibria has been performed with the VMEC code [4]. The convergence parameter (ftol) has been fixed to $10^{-11}$. The number of surfaces, poloidal mesh and toroidal mesh have been fixed to 100, 30 and 20, respectively, except for the convergence study of $\nabla \cdot \mathbf{j}$ in section 6, where the highest poloidal mode number $m_x$ and the poloidal mesh were varied. The number of surfaces of the precursor runs in VMEC has been fixed to 41. The total number of modes used for the equilibrium calculation was 61 ($0 \leq m_x \leq 5$, $-5 \leq n_x/L \leq 5$, where $n_x$ is the toroidal mode number and $L$ is the period number of the device).

The equilibrium reconstruction in Boozer coordinates and the Mercier criterion have been obtained with the mapping routines of the TERPSICHORE code [5]. One needs 186 mode pairs in which the amplitudes are significant for the equilibrium reconstruction in Boozer coordinates [6]. For the ballooning stability analysis, the spectrum of modes required must be increased to 681, with the poloidal mode number $m$ approaching 60. These values are large enough to guarantee the reliability of the results.

# 3 The two calculation methods for the parallel current

Boozer coordinates [7] are used because they allow a very precise representation of the $\mathbf{B}\cdot\nabla$ operator and the parallel current density ($\mathbf{j}\cdot\mathbf{B}/B^2$). In this coordinate system, the magnetic field in the contravariant representation is given by

$$\mathbf{B} = \nabla\phi \times \nabla\Psi + \nabla\Phi \times \nabla\theta, \tag{1}$$

and in the covariant representation by

$$\mathbf{B} = B_s\nabla s + J(s)\nabla\theta - I(s)\nabla\phi \tag{2}$$

where $\Psi(s)$ is the poloidal flux function, $\Phi(s)$ is the toroidal flux function, $I(s)$ is the poloidal current flux function, $J(s)$ is the toroidal current flux function and $B_s$ is the radial covariant component of $\mathbf{B}$.

The dot product of the two representations for the magnetic field yields

$$\sqrt{g}B^2 = \Psi'(s)J(s) - \Phi'(s)I(s) \tag{3}$$

where $\sqrt{g}$ is the Jacobian of the transformation and a prime means a derivative with respect to $s$.

The parallel current density constitutes an important driving mechanism for MHD instabilities in 3D configurations [8]. Therefore, the question of how it is computed is a critical issue in the determination of beta limits imposed by MHD. The relation between the parallel current density and $B_s$ is given by

$$\left(\frac{\mathbf{j}\cdot\mathbf{B}}{B^2}\right) = \frac{1}{\sqrt{g}B^2}\left[\left(\frac{\partial B_s}{\partial \phi} - \frac{\partial B_\phi}{\partial s}\right)B_\theta + \left(\frac{\partial B_\theta}{\partial s} - \frac{\partial B_s}{\partial \theta}\right)B_\phi\right]. \tag{4}$$

There are two methods to calculate $B_s$: the magnetic method, where we invoke the radial component of the MHD force balance relation, given by

$$\sqrt{g}p'(s) + \Psi'(s)J'(s) - \Phi'(s)I'(s) = \sqrt{g}\mathbf{B}\cdot\nabla B_s \tag{5}$$

and the geometric method, given by

$$B_s = \frac{1}{\sqrt{g}}\left(g_{s\theta}\Psi'(s) + g_{s\phi}\Phi'(s)\right) \tag{6}$$

where $g_{s\theta}$ and $g_{s\phi}$ are the metric tensor components. Once $B_s$ is determined, we calculate $(\mathbf{j}\cdot\mathbf{B}/B^2)$ according to Eq. 4. It is straightforward to demonstrate that the evaluation of the flux-surface varying component of the parallel current density with the magnetic method of Eqs. 4 and 5 is equivalent to its determination through the application of charge conservation, $\nabla\cdot\mathbf{j} = 0$, and MHD force balance.

# 4 The marginal beta values for stability

A previous estimate of the maximal average beta value guaranteeing ballooning and Mercier stability for the whole plasma in the W 7-X configuration has already been obtained in Reference [9]. Figure 2 shows the marginal values of beta as a function of the flux surfaces. One sees that the ballooning stability is more restrictive than the Mercier criterion. The figure shows a localized instability around the resonant surface $\iota_p = 2/11$ ($\iota_p$ means iota per period). This instability, like all instabilities at rational surfaces except the $\iota_p = 1/6$, exists in the plasma for values of beta much smaller than 5%. Nührenberg showed that these instabilities are localised enough [2], that when the pressure gradient is made to vanish at the resonant surface, one can be sure that this surface is stable with respect to the Mercier criterion. Therefore, flattening the pressure profile very locally can assure stability at these rational surfaces.

As shown in section 6, the Mercier criterion calculated with the geometric method always predicts stability. Therefore, the Mercier criterion has been calculated with the magnetic method to obtain the marginal beta values as a function of the radial variable that labels the flux surfaces.

Finally, we found that the highest beta value guaranteeing local stability in the whole plasma is given by $\beta = 5.07\%$.

# 5 The ballooning stability

To obtain the 3D ballooning equation, one minimises the energy principle using the covering space concept [11]. Transforming in Boozer coordinates, one obtains

$$\frac{\partial}{\partial\theta}\left\{[C_p + C_s(\theta-\theta_k) + C_q(\theta-\theta_k)^2]\frac{\partial\chi}{\partial\theta}\right\} + (1-\lambda)[d_p + d_s(\theta-\theta_k)]\chi = 0 \quad (7)$$

where the coefficients are given by [12]

$$C_p = \left[\frac{g_{ss}}{\sqrt{g}} - \frac{B_s^2}{\sqrt{g}B^2}\right], \quad (8)$$

$$C_s = 2\,\frac{q'(s)\Psi'(s)}{\Phi'(s)}\left[\frac{J(s)B_s}{\sqrt{g}B^2} - \frac{g_{s\theta}}{\sqrt{g}}\right], \quad (9)$$

$$C_q = \frac{[q'(s)\Psi'(s)]^2}{\sqrt{g}B^2}\,|\nabla s|^2, \quad (10)$$

$$d_p = \frac{p'(s)}{[\Psi'(s)]^2}\left[\frac{\sqrt{g}\,p'(s)}{B^2} + \frac{[J(s)\Psi''(s) - I(s)\Phi''(s)]}{B^2} - \frac{\partial\sqrt{g}}{\partial s} + \sqrt{g}\,\mathbf{B}\cdot\nabla\left(\frac{B_s}{B^2}\right)\right], \quad (11)$$

$$d_s = -\frac{q'(s)}{\Psi'(s)}\sqrt{g}\,\mathbf{B}\cdot\nabla\left(\frac{\mathbf{j}\cdot\mathbf{B}}{B^2}\right) \quad (12)$$

where we identify $\theta_k$ as the radial wave number [10] and $q(s)$ is the inverse of the total rotational transform iota.

Figure 3 shows a typical result of the eigenvalue with respect to the surface for a given value of beta. If the eigenvalue is positive, then the surface is unstable. For the ballooning calculations, we impose the condition that the eigenstructures along the magnetic field lines should vanish within 30 poloidal transits around the plasma. Therefore, the coefficients $d_p$ and $d_s$ do not fully sense the singular nature of the parallel current density in the vicinity of mode rational surfaces. Although the coefficients $C_p$ and $C_s$ explicitly contain the function $B_s$ which becomes singular at mode rational surfaces (using the magnetic method), this does not affect the ballooning results. To illustrate this, we plot the field line bending term, $C_p + C_s(\theta-\theta_k) + C_q(\theta-\theta_k)^2$, on the closest field line approaching the $\iota_p = 1/6$ resonance (at $s = 0.1465$) in Fig. 4a and on another field line at some distance from the resonance (at $s = 0.1768$) in Fig. 4b, with $\theta_k = 0$. The basic structure and the magnitude of the field line bending term is unaltered by the behaviour of $B_s$. The corresponding ballooning eigenstructures are presented in Figs. 5a and 5b, respectively.

# 6 The Mercier criterion

The Mercier criterion can be derived from the asymptotic analysis (in the limit $y = \theta - \theta_k \to \infty$) [13] of the ballooning mode equation. Retaining the ballooning

eigenvalue as part of the analysis, the Mercier criterion can be expressed in the form [12]

$$\lambda = 1 + \frac{D_1}{2D_2} - \frac{(D_1^2 + D_2)^{1/2}}{2D_2} \leq 0 \tag{13}$$

for stability, with

$$D_1 = \langle h_q \rangle \langle d_p \rangle - \langle h_q \rangle \langle d_q \rangle + \langle h_q d_q \rangle, \tag{14}$$

$$D_2 = \langle h_q \rangle \langle h_q d_q^2 \rangle - \langle h_q d_q \rangle^2 \tag{15}$$

where we have defined the average

$$\langle f \rangle \equiv \frac{L}{(2\pi)^2} \int_0^{2\pi/L} d\phi \int_0^{2\pi} d\theta f(s, \theta, \phi). \tag{16}$$

The relevant coefficients are

$$h_q = \frac{1}{C_q} = \frac{\sqrt{g} B^2}{[q'(s)\Psi'(s)]^2 |\nabla s|^2}, \tag{17}$$

$$d_q = -q'(s) \left( \frac{\mathbf{j} \cdot \mathbf{B}}{B^2} \right). \tag{18}$$

One can see that the Mercier criterion depends directly on the parallel current density via Eq. 18. A typical result of our study is shown in Figure 6 where we represent the value of the Mercier criterion (expressed as $-\lambda$) with respect to iota. One can see first that the geometric method is not sensitive to resonant surfaces. To understand this, we consider the Fourier components of the parallel current density as calculated by the magnetic method. Using the condition of charge conservation, $\nabla \cdot \mathbf{j} = 0$, we find

$$\left( \frac{\mathbf{j} \cdot \mathbf{B}}{B^2} \right)_{m,n}^{magn} = \left[ \frac{p'(s)}{\Psi'(s)J(s) - \Phi'(s)I(s)} \right] \left[ \frac{mI(s) - nJ(s)}{m\Psi'(s) - n\Phi'(s)} \right] (\sqrt{g})_{m,n} \tag{19}$$

for all the components except the $m = 0$, $n = 0$ contribution. The geometric method gives (except $m = 0$, $n = 0$)

$$\left( \frac{\mathbf{j} \cdot \mathbf{B}}{B^2} \right)_{m,n}^{geom} = \left[ \frac{mI(s) - nJ(s)}{\Psi'(s)J(s) - \Phi'(s)I(s)} \right] (B_s)_{m,n} \tag{20}$$

with $B_s$ calculated according to Eq. 6. There is an explicit singularity with the magnetic method at every rational surface which is not the case for the geometric method.

The second observation that we have made is that there is a difference between the two methods for nonresonant surfaces too. Gardner and Blackwell mentioned also this problem in their paper [3]. We believe that the reason for this difference is that the truncation of the Fourier spectrum in the equilibrium calculation causes the geometric method to violate the condition $\nabla \cdot \mathbf{j} = 0$. The magnetic method uses this condition explicitly to determine the parallel current density, but the geometric method does not. One can write $\nabla \cdot \mathbf{j}$ in Fourier space as

$$\begin{aligned} (\sqrt{g} \nabla \cdot \mathbf{j})_{m,n} &= \frac{p'(s)}{\sqrt{g} B^2} [mI(s) - nJ(s)] (\sqrt{g})_{m,n} \\ &\quad - [m\Psi'(s) - n\Phi'(s)] \left( \frac{\mathbf{j} \cdot \mathbf{B}}{B^2} \right)_{m,n} = 0. \end{aligned} \tag{21}$$

One can see that this condition is always verified for the magnetic method, by substituting Eqs. 3 and 19 into Eq. 21. Using the geometric method, we obtain

$$(\sqrt{g}\nabla\cdot\mathrm{j})^{geom}_{m,n} = [m\Psi'(s) - n\Phi'(s)]\left[\left(\frac{\mathrm{j}\cdot\mathrm{B}}{B^2}\right)^{magn}_{m,n} - \left(\frac{\mathrm{j}\cdot\mathrm{B}}{B^2}\right)^{geom}_{m,n}\right] = 0. \quad (22)$$

It is worthwhile to note that the factor $[m\Psi'(s) - n\Phi'(s)]$ annihilates the error in the calculation of $\nabla\cdot\mathrm{j}$ at the resonant surface in Eq. 22. Consequently, Eq. 22 constitutes a useful measure of the error in the computation of $\nabla\cdot\mathrm{j}$ at a distance from the resonant layer. Figure 7 shows that the condition given by Eq. 22 is not respected.

We have performed a convergence study of $\sqrt{g}\nabla\cdot\mathrm{j}$ with respect to the maximum poloidal mode number $m_x$ used in the computation of the equilibria with VMEC. It is very difficult to get $m_x$ higher than 16, because the equilibrium begins to converge poorly near the magnetic axis. However, Figure 8 shows that the convergence seems to vary between $1/m_x^{1/3}$ and $1/m_x^{1/2}$. This slow rate of convergence implies that the geometric method for determining the parallel current density is ineffective for the accurate determination of the Mercier criterion. Therefore, we can say that there is a systematic error in the parallel current density calculated with the geometric method, when the spectrum of modes used to calculate the equilibrium is truncated at a low number.

# 7 Conclusions

We confirm the volume average $\beta$ limit of 5% predicted for the W 7-X device. Ballooning stability in W 7-X does not depend on how $(\mathrm{j}\cdot\mathrm{B}/B^2)$ is calculated because these modes are localized along the field lines. Therefore the ballooning modes are not sensitive to the singular behaviour of the parallel current density in the vicinity of rational surfaces. The Mercier modes, being extended structures along the field lines, depend sensitively on the method of determination of $(\mathrm{j}\cdot\mathrm{B}/B^2)$. The discrepancy between the two methods extends beyond low order rational surfaces because the truncation of the Fourier spectrum in the computation of the equilibrium state causes the condition $\nabla\cdot\mathrm{j} = 0$ to be violated for cases in which the geometric method is applied to calculate $(\mathrm{j}\cdot\mathrm{B}/B^2)$.

# Acknowledgements

This work was partly supported by the Swiss National Science Foundation and by Euratom. We thank J. Nührenberg for suggesting the study of the convergence properties of the parallel current density with the spectrum of modes employed in the equilibrium calculation. We also thank S. P. Hirshman for providing us with the VMEC code.

# References

[1] **Lotz W., Nührenberg J. and Schwab C.**, in *Proc. 13th Int. Conf. on Plasma Physics and Contr. Nucl. Fusion Research* (Washington, 1990), IAEA (Vienna, 1991) Vol. II, 603.

[2] Nührenberg J. and Zille R., *Physics Letters* **114A** (1986) 129.

[3] Gardner H. J. and Blackwell B. D., *Nucl. Fusion* **32** (1992) 2009.

[4] Hirshman S. P. and Betancourt O., *J. Comput. Phys.* **96** (1991) 99.

[5] Anderson D. V., Cooper W. A., Gruber R., Merazzi S. and Schwenn U., *Int. J. Supercomp. Appl.* **4** (1990) 34.

[6] Cooper W. A., Fu G. Y., Schwab C., Schwenn U., Gruber R., Merazzi S. and Anderson D. V., in *Proc. 13th Int. Conf. on Plasma Physics and Contr. Nucl. Fusion Research* (Washington, 1990), IAEA (Vienna, 1991) Vol. II, 793.

[7] Boozer A. H., *Physics Fluids* **23** (1980) 904.

[8] Nührenberg J. and Zille R., in *Proc. of the Workshop on Theory of Fusion Plasmas,* EUR 11336 EN (1987), pp. 3-23. Editrice Compositori, Bologna.

[9] Beidler C., Grieger G., Herrnegger F., Harmeyer E., Kisslinger J., Lotz W., Maassberg H., Merkel P., Nührenberg J., Rau F., Sapper J., Sardei F., Scardovelli R., Schlueter A. and Wobig H., *Fusion Technology* **17** (1990) 148.

[10] Correa-Restrepo D., *Z. Naturforsch.* **33a** (1978) 789.

[11] Dewar R. L. and Glasser A. H., *Physics Fluids* **26** (1983) 3038.

[12] Cooper W.A., *Plasma Physics and Controlled Fusion* **34** (1992) 1011.

[13] Connor J. W., Hastie J. and Taylor J. B., *Proc. R. Soc. London,* **A365** (1979) 1.

# The figures captions

- Figure 1 : The normalised pressure profile. This nearly optimal profile becomes marginally stable to localised ideal MHD modes almost uniformly throughout the plasma.
- Figure 2 : The maximal average beta value guaranteeing local stability for the W 7-X configuration. The solid line represents the beta limit for the ballooning stability calculated with the magnetic method and the dotted line the beta limit for the ballooning stability when the geometric method is used. The short dashed line represents the beta limit for the Mercier stability criterion connected with the $\iota_p = 1/6$ rational surface and the large dashed line represents an example of a local instability due to a rational surface other than $\iota_p = 1/6$ (here $\iota_p = 2/11$). The maximal beta value allowing local stability for the whole plasma is given by $\beta = 5.07\%$.
- Figure 3 : An example of a typical result for ballooning stability. The solid (dotted) line represents the ballooning eigenvalue calculated with the magnetic (geometric) method for $\beta = 6.46\%$. A surface is stable if the eigenvalue is negative. One can see that the two methods of calculation of the parallel current density give the same result for the main part of the plasma.
- Figure 4a : The field line bending term $C_p + C_s(\theta - \theta_k) + C_q(\theta - \theta_k)^2$ as a function of the values of $\theta$ along a magnetic field line $\alpha = \phi - q(s)\theta = 0$ on the surface $s = 0.1465$ near the $\iota_p = 1/6$ resonance.
- Figure 4b : The field line bending term $C_p + C_s(\theta - \theta_k) + C_q(\theta - \theta_k)^2$ as a function of the values of $\theta$ along a magnetic field line $\alpha = \phi - q(s)\theta = 0$ on the surface $s = 0.1768$.
- Figure 5a : The ballooning eigenfunction versus the values of $\theta$ along a magnetic line ($\alpha = \phi - q(s)\theta = 0$) at $s = 0.1465$.
- Figure 5b :The ballooning eigenfunction versus the values of $\theta$ along a magnetic line ($\alpha = \phi - q(s)\theta = 0$) at $s = 0.1768$.
- Figure 6 : An example of the value of the Mercier criterion (expressed as $-\lambda$) calculated with the magnetic (solid line) or the geometric (dotted line) method. The value of beta is 7.94% here. A surface is stable if the Mercier criterion is positive. The geometric method is not sensitive to the rational surfaces. In contrast, one can see instabilities due to the $\iota_p = 1/6$ and $\iota_p = 2/11$ rational surfaces for the Mercier criterion calculated with the magnetic method. The two methods do not give the same results for nonrational surfaces either.
- Figure 7 : The $m = 6$, $n = 1$ Fourier space component of $\sqrt{g}\nabla \cdot \mathbf{j}$ calculated with the geometric method. The solid, dotted, short dashed and long dashed lines correspond to the maximum poloidal mode number used in the computation of the equilibria with VMEC, $m_x = 6$, $m_x = 8$, $m_x = 12$ and $m_x = 16$, respectively. The number of surfaces is 50 here. The figure shows that the condition of charge conservation is violated when the geometric method is used. The ragged structure of the $m_x = 16$ curve is symptomatic of incipient convergence difficulties in the computation of the equilibrium state.

- Figure 8 : Convergence study of the $m = 6$, $n = 1$ Fourier space component of $\sqrt{g}\nabla \cdot \mathbf{j}$ calculated with the geometric method. The solid line represents the surface $s = 0.96$, the dotted line the surface $s = 0.8$ and the dashed line the surface $s = 0.7$. The convergence seems to vary between $1/m_x^{1/3}$ and $1/m_x^{1/2}$. It is difficult to get results for a value of $m_x$ higher than 16 because the equilibrium begins to converge poorly near the magnetic axis.

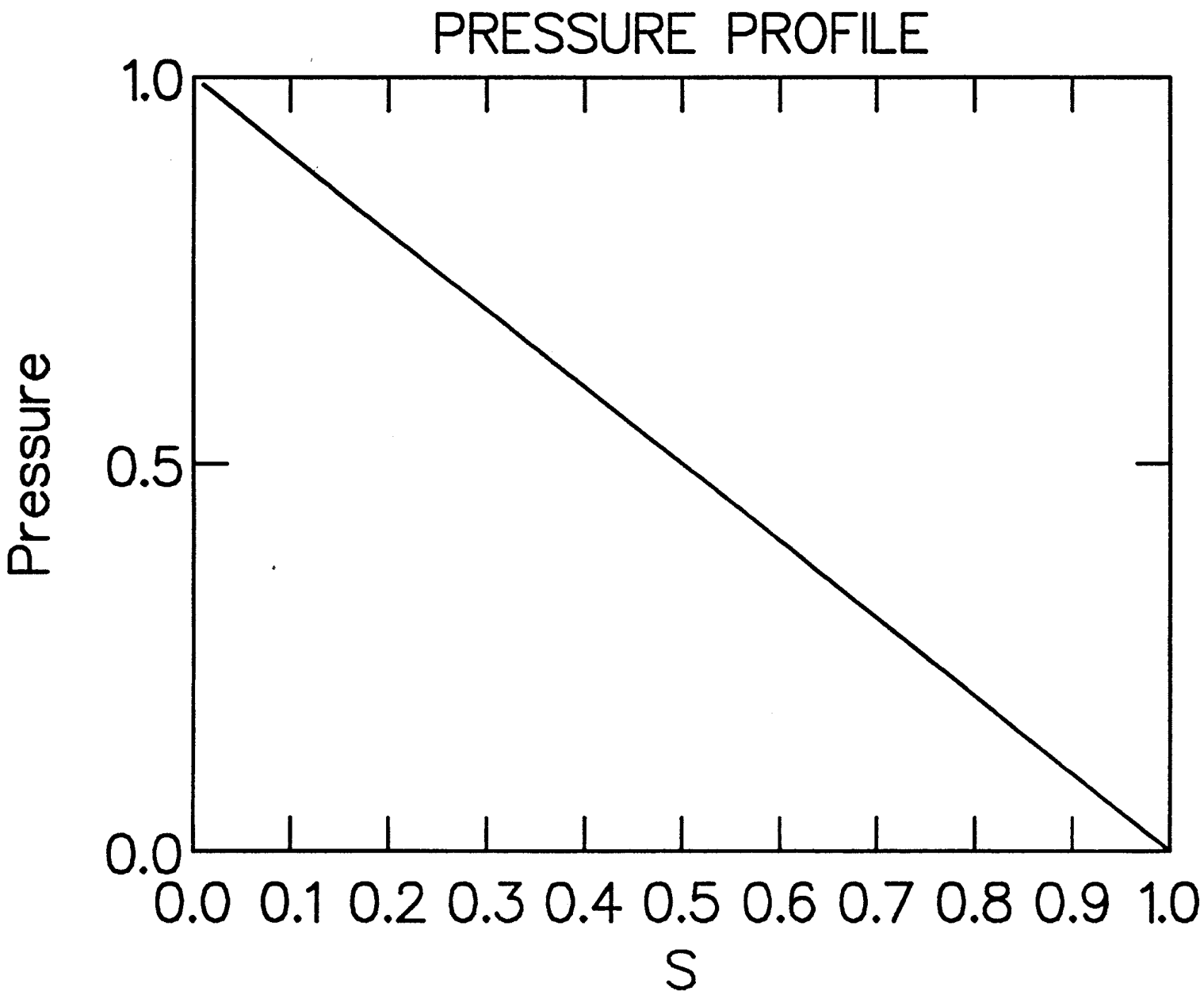
PRESSURE PROFILE
Pressure
1.0
0.5
0.0
0.0 0.1 0.2 0.3 0.4 0.5 0.6 0.7 0.8 0.9 1.0
S

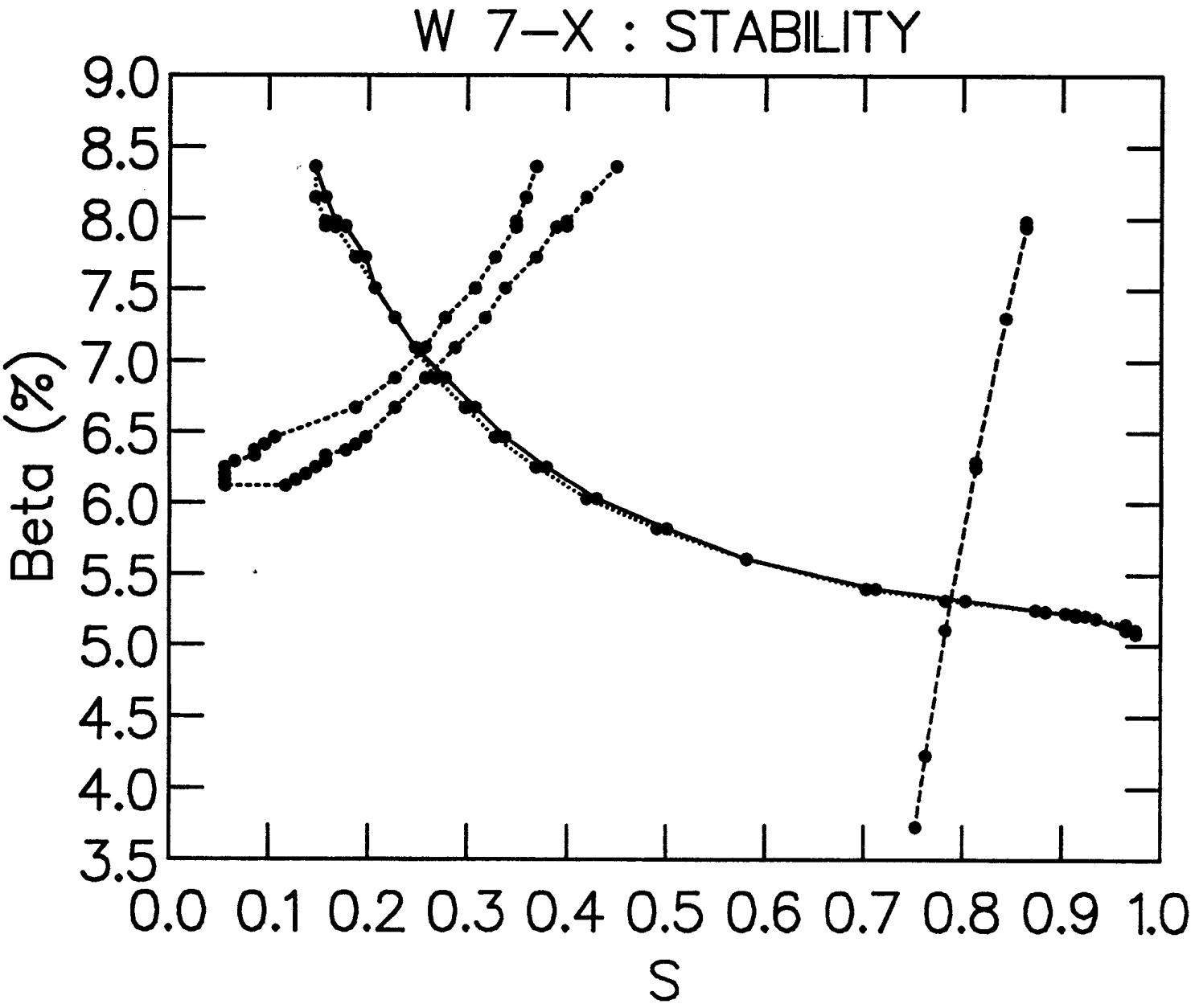
W 7–X : STABILITY
Beta (%)
9.0
8.5
8.0
7.5
7.0
6.5
6.0
5.5
5.0
4.5
4.0
3.5
0.0 0.1 0.2 0.3 0.4 0.5 0.6 0.7 0.8 0.9 1.0
S

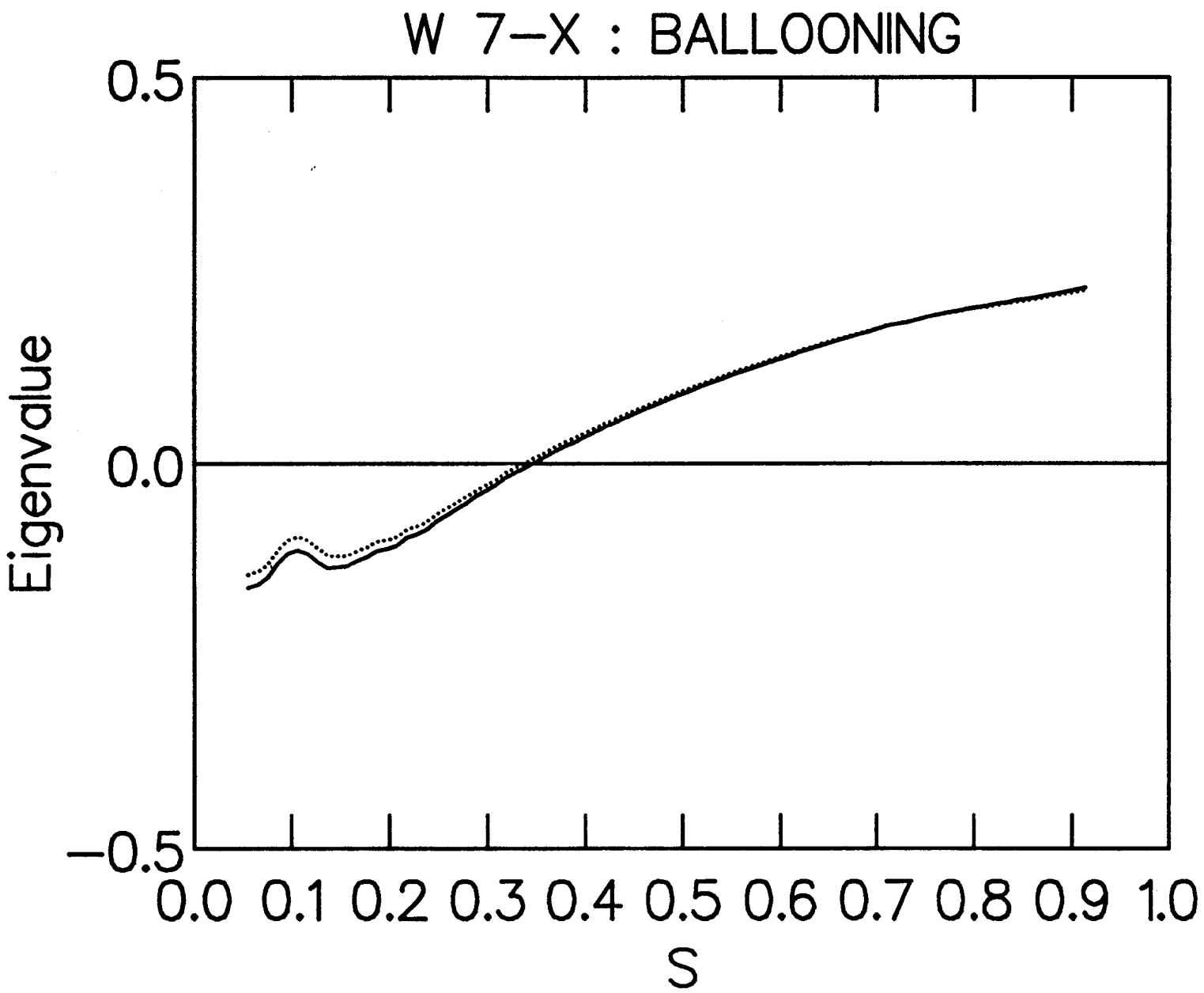
W 7–X : BALLOONING
0.5
0.0
−0.5
Eigenvalue
0.0 0.1 0.2 0.3 0.4 0.5 0.6 0.7 0.8 0.9 1.0
S

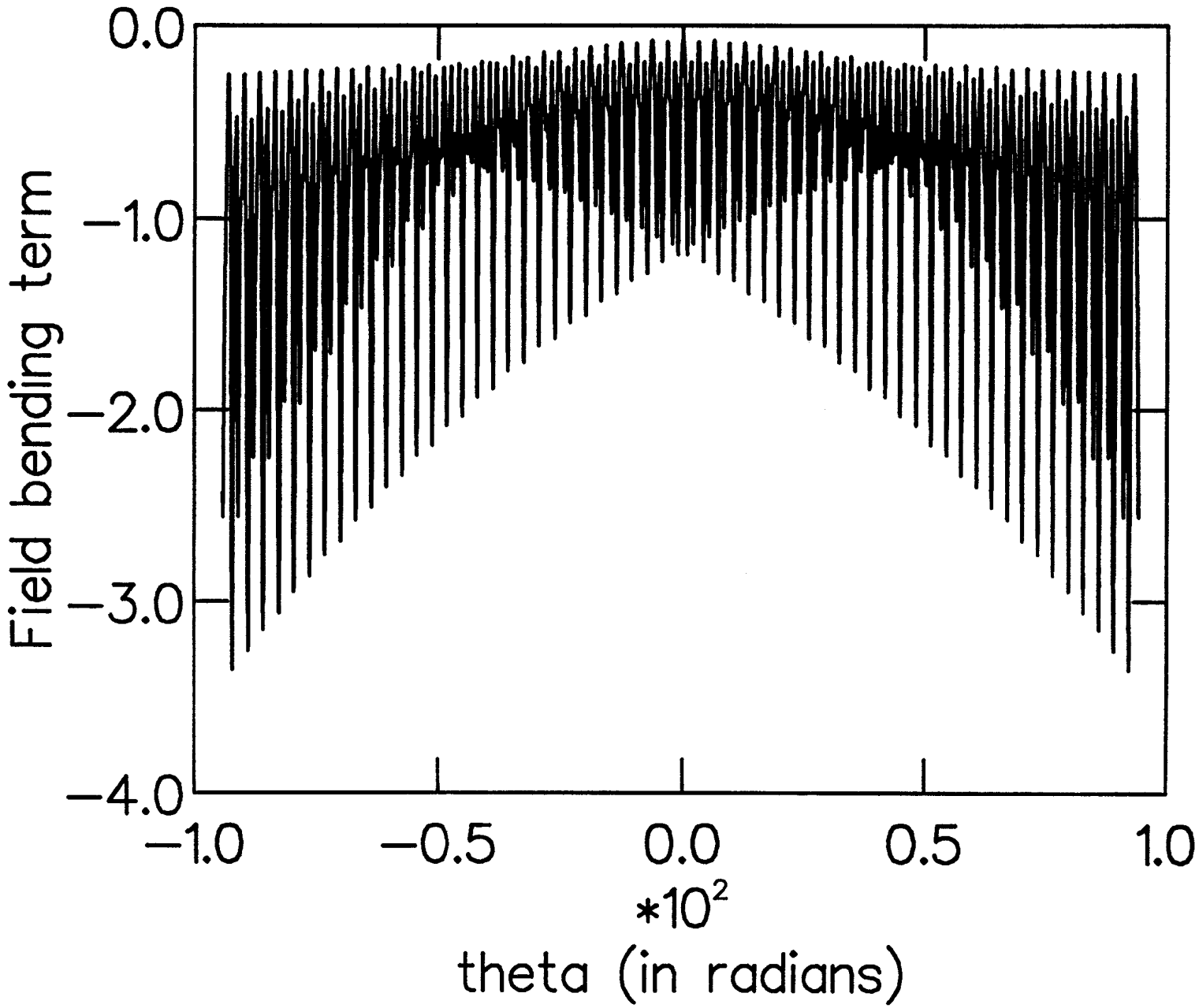
0.0
−1.0
−2.0
−3.0
−4.0
Field bending term
−1.0
−0.5
0.0
0.5
1.0
*10²
theta (in radians)

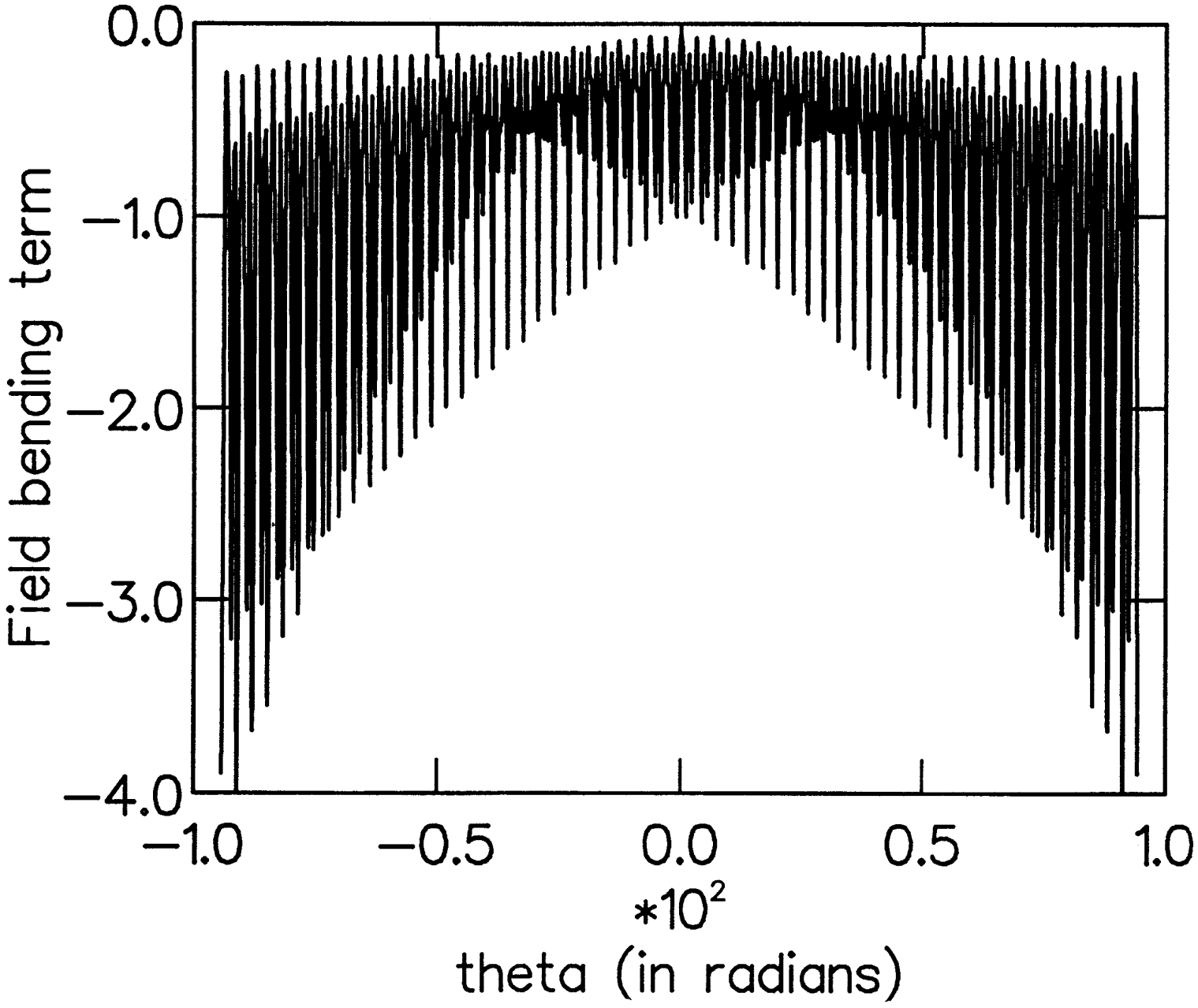
0.0
−1.0
−2.0
−3.0
−4.0
Field bending term
−1.0
−0.5
0.0
0.5
1.0
*10²
theta (in radians)

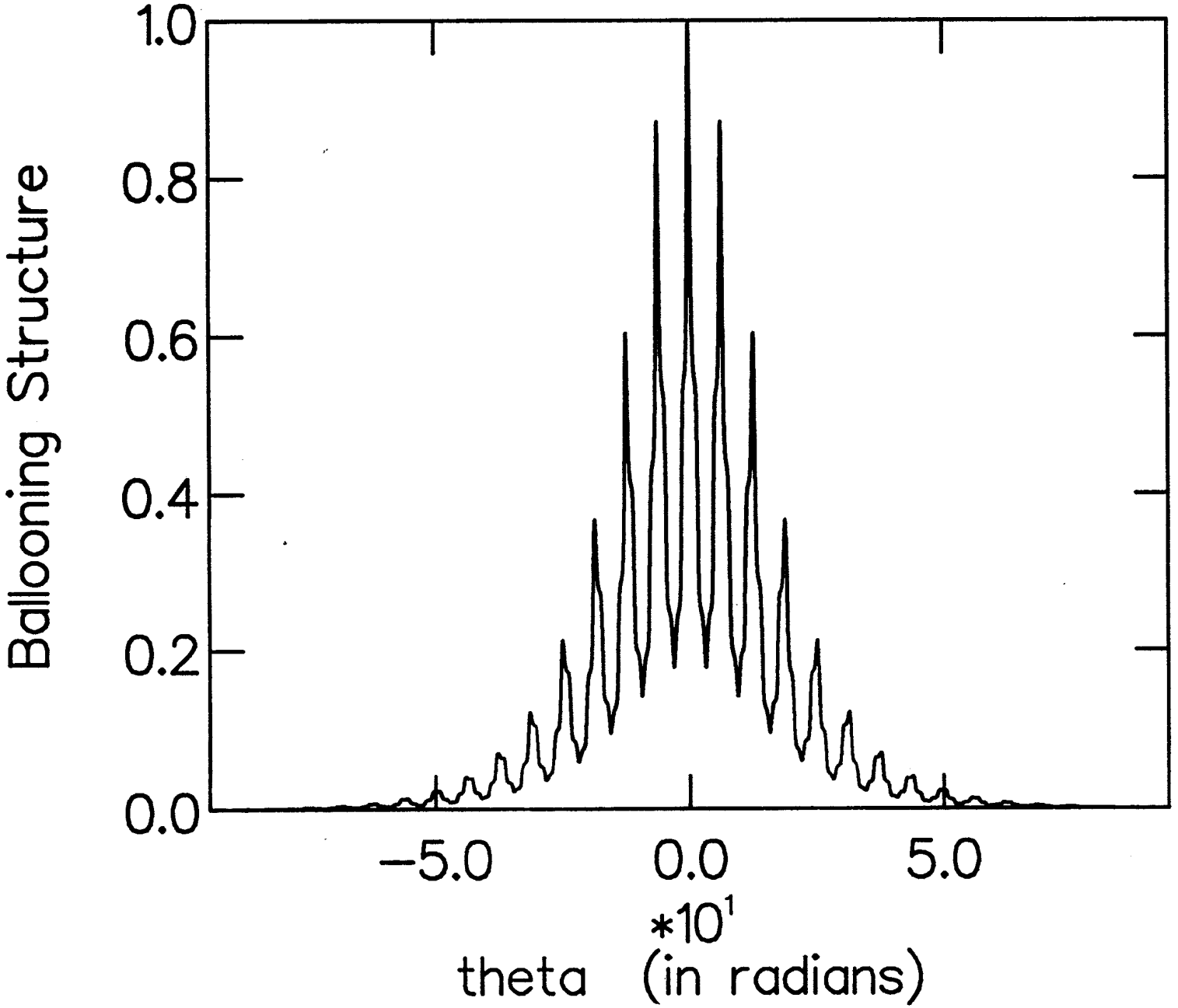
Ballooning Structure
1.0
0.8
0.6
0.4
0.2
0.0
−5.0
0.0
5.0
*10^1
theta (in radians)

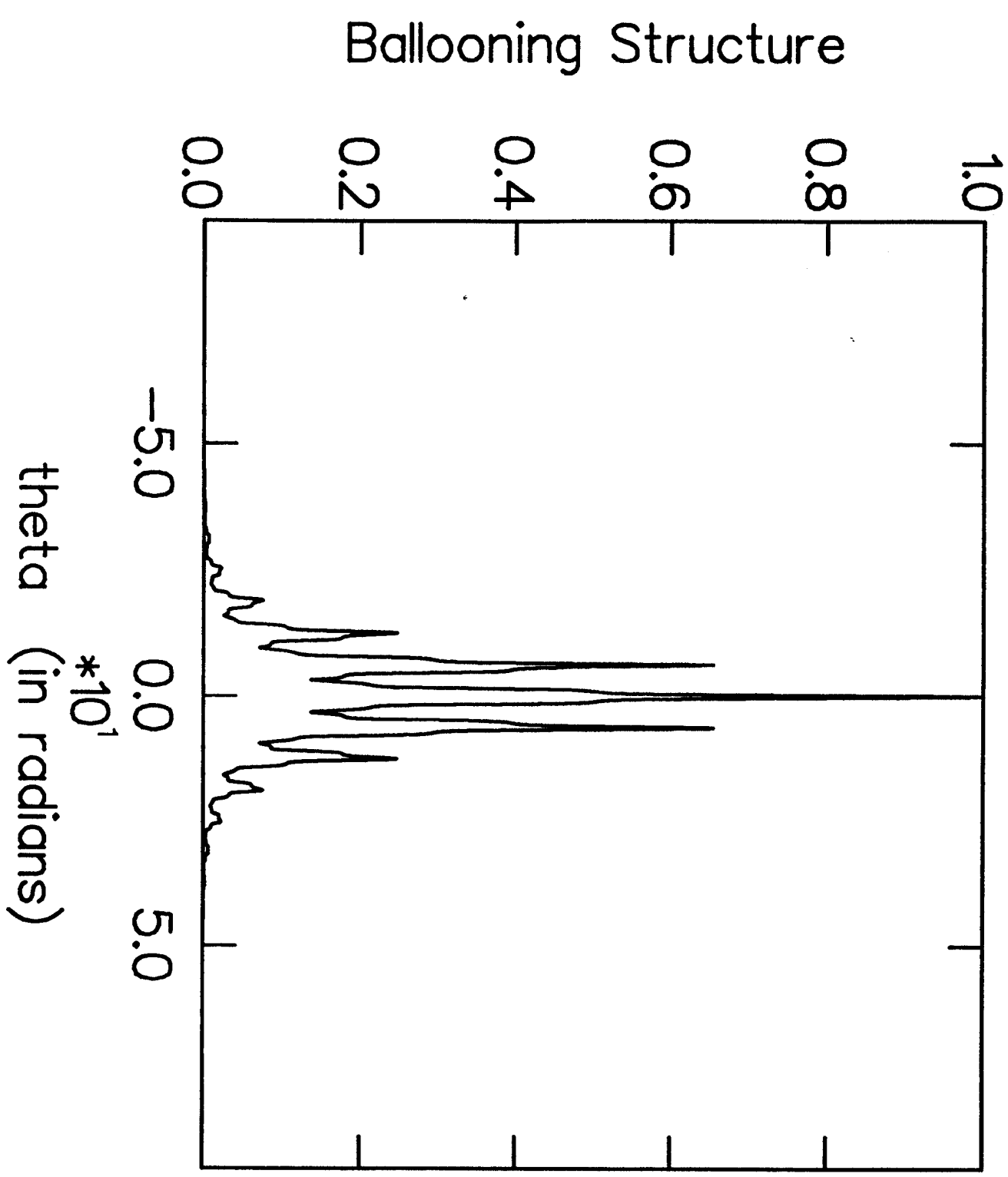
Ballooning Structure
0.0
0.2
0.4
0.6
0.8
1.0
-5.0
0.0
5.0
theta (in radians)
*10^1

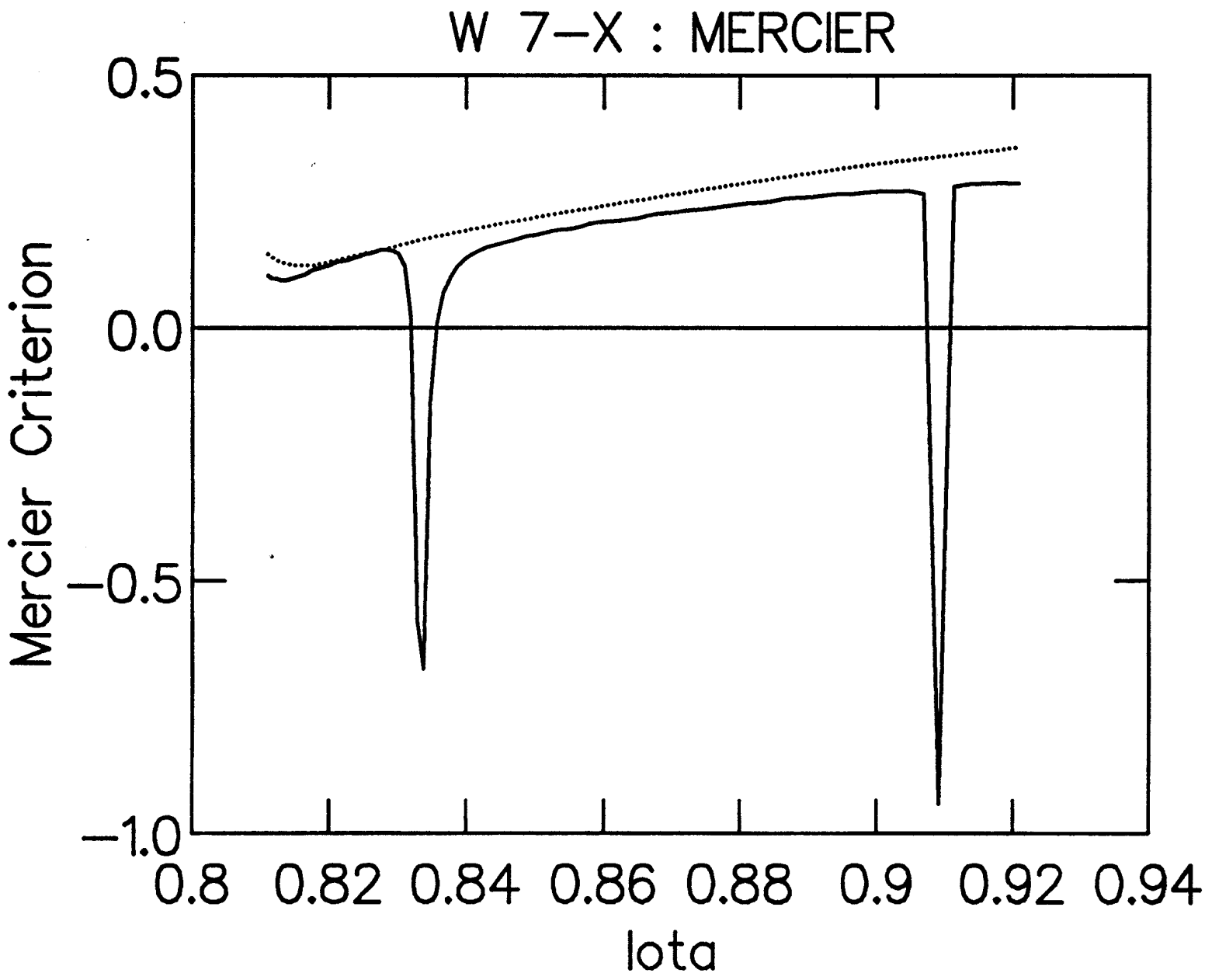
W 7-X : MERCIER
0.5
0.0
−0.5
−1.0
Mercier Criterion
0.8
0.82
0.84
0.86
0.88
0.9
0.92
0.94
Iota

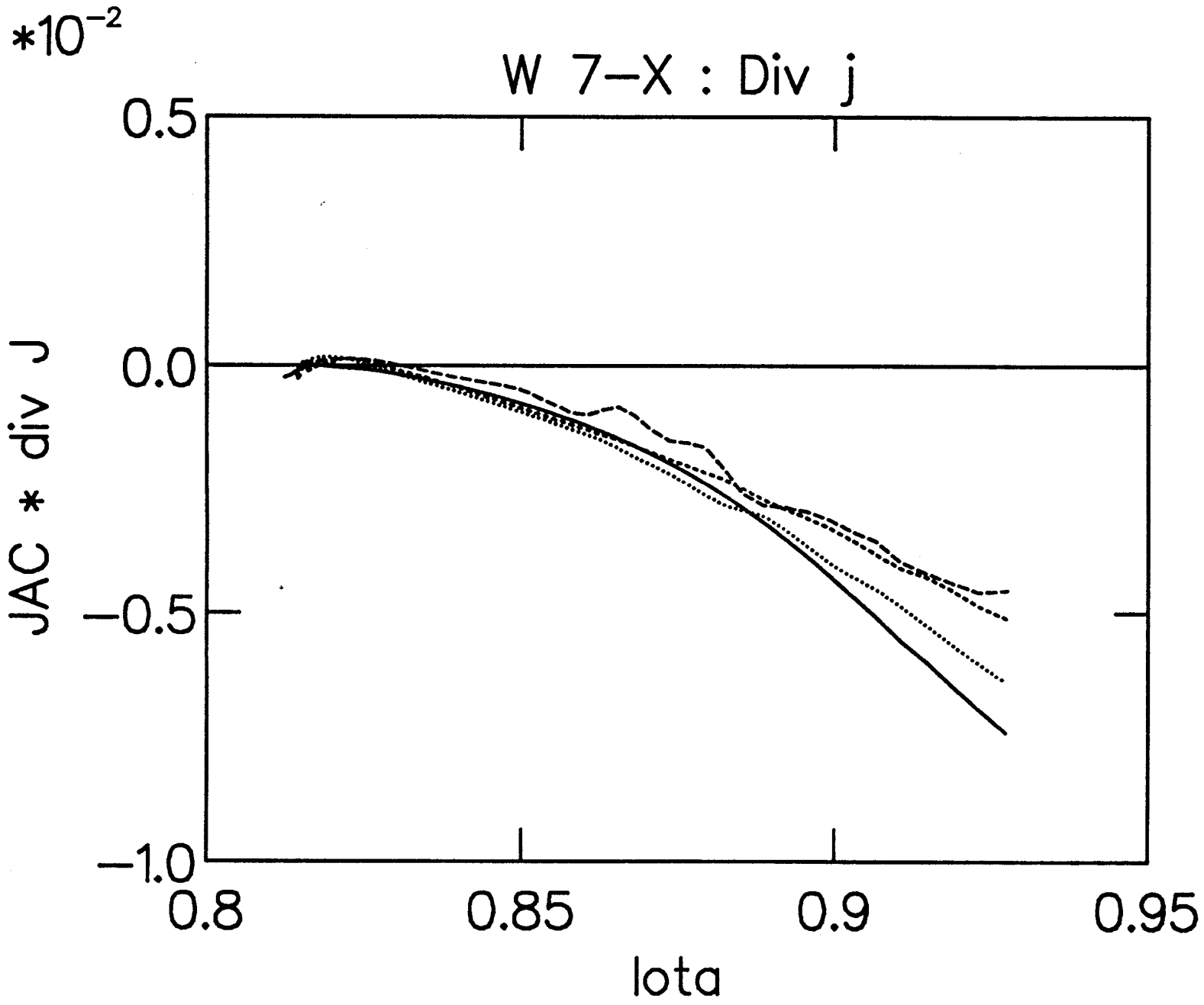
*10^-2
W 7-X : Div j
0.5
0.0
-0.5
-1.0
JAC * div J
0.8
0.85
0.9
0.95
Iota

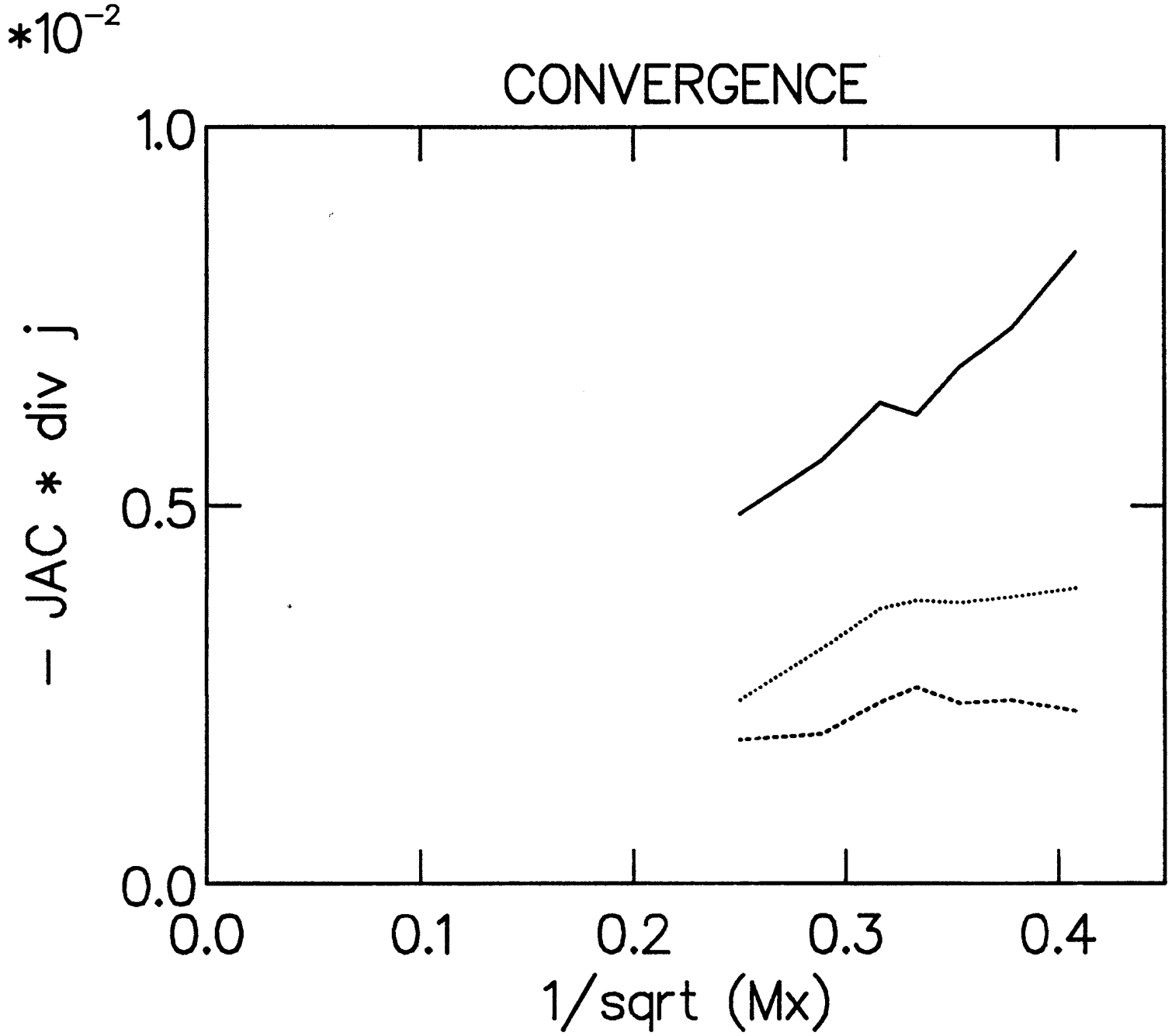
*10^-2
CONVERGENCE
1.0
0.5
0.0
- JAC * div j
0.0
0.1
0.2
0.3
0.4
1/sqrt (Mx)